Applied Microscopy

RESEARCH

Open Access

In-situ formation of co particles encapsulated by graphene layers

Minjeong Lee[1], Gyutae Kim[1], Gyu Hyun Jeong[1], Aram Yoon[2,3], Zonghoon Lee[2,3] and Gyeong Hee Ryu[1*]

Abstract

The process of encapsulating cobalt nanoparticles using a graphene layer is mainly direct pyrolysis. The encapsulation structure of hybrids prepared in this way improves the catalyst stability, which greatly reduces the leaching of non-metals and prevents metal nanoparticles from growing beyond a certain size. In this study, cobalt particles surrounded by graphene layers were formed by increasing the temperature in a transmission electron microscope, and they were analyzed using scanning transmission electron microscopy (STEM). Synthesized cobalt hydroxide nanosheets were used to obtain cobalt particles using an in-situ heating holder inside a TEM column. The cobalt nanoparticles are surrounded by layers of graphene, and the number of layers increases as the temperature increases. The interlayer spacing of the graphene layers was also investigated using atomic imaging. The success achieved in the encapsulation of metallic nanoparticles in graphene layers paves the way for the design of highly active and reusable heterogeneous catalysts for more challenging molecules.

Keywords: Co particle, Encapsulation, Graphene, Co $(OH)_2$, STEM

Introduction

Metallic catalysts play a dominant role in industrial applications and the development of catalysts using base metals (Jagadeesh et al. 2013a; Meffere et al. 2015; Jagadeesh et al. 2013b; Czaplik et al. 2007; Zhang et al. 2013) is prevalent because of their distinct electronic structures (Friedfeld et al. 2013) and magnetic properties. In addition, a series of novel heterogeneous catalyst systems using noble metal catalysts (Rahi et al. 2012; Le et al. 2013; Ren et al. 2012; Yan et al. 2013; Ge et al. 2013) have been developed, but noble metals have major drawbacks such as lack of selectivity and low resistance to functional groups (Corma et al. 2008).

In recent years, multi-metal catalysts made by bonding different transition metals have come into prominence (Sammis et al. 2004; Toyofuku et al. 2008; Hashmi et al. 2009; Chinchilla et al. 2007). The driving force behind these efforts is the discovery of more efficient approaches for the synthesis of complex molecules with superior chemical and stereoselectivity that are not accessible through the use of monospecific catalyst systems. The development of these catalysts maximized compatibility while exploiting the benefits of catalysis. Furthermore, transition metals are predominantly applied to find more valuable chemical transformations. This growing interest has led to advances in the field focusing on how the reactivity of transition metal catalysts can be tuned. In addition to this, a strategy has been derived to create metal nanoparticles encapsulated in polymorphic carbon shells (Yao et al. 2014; Galakhov et al. 2010; Liu et al. 2011). The main advantage of encapsulated structures is the ability to tune the electronic structure of metal nanoparticles and tightly control the aggregation of nanoparticles (Chen et al. 2014; Tian et al. 2015). In addition, encapsulation of

*Correspondence: gh.ryu@gnu.ac.kr

[1] School of Materials Science and Engineering, Gyeongsang National University, Jinju 52828, Republic of Korea
Full list of author information is available at the end of the article

metal nanoparticles within a porous carbon shell allows for easy access to the catalytically active sites and greatly inhibits mass transfer restrictions (Wu et al. 2014).

Recently, Co encapsulated in a carbon matrix has been developed for various reactions such as catalytic hydrogenation and ORR (Wei et al. 2016; Liu et al. 2015; Yang et al. 2018; Wei et al. 2015). Hybrid Co particles specifically designed to be encapsulated in a carbon material serve as an efficient, selective, and potent catalyst. The interface between the encapsulated Co particles and the graphene layer determines the structural and chemical properties. For metal/graphene systems, interfaces have also been focused on applying graphene to electronic devices where graphene is in contact with metal electrodes and wires (Rosei et al. 1984; Nagashima et al. 1994; Gamo et al. 1997; Abild-Pedersen et al. 2006; Wang et al. 2007; Gruneis et al. 2008). Because these Co/graphene interfaces are two-dimensional internal structures, transmission electron microscopy (TEM) is the most useful method to investigate them. Herein, we report the formation of Co particles encapsulated by graphene layers, which were induced using an in-situ TEM heating holder in a TEM column. We used synthesized Co $(OH)_2$ nanosheets and converted them into Co particles. The carbon matrix, which remained amorphous, was transformed into graphene layers surrounding the Co particles at high temperatures (over 800 °C). Interestingly, the number of graphene layers increases when heated to above 1000 °C. The whole process was analyzed using high-resolution STEM.

Results and discussion

Figure 1a shows a encapsulation process of co particle when we have experiment using Co $(OH)_2$ nanosheets. We deal with a detailed explanation of the process sequentially. Cobalt hydroxide can be synthesized as nanosheets as shown in Fig. 1b. Their chemical bonding states were confirmed using x-ray photoelectron spectroscopy (XPS) to consist of mainly cobalt hydroxide with some cobalt oxides (Fig. 1c). The peak of O1s at 531.1 eV indicates that the Co atoms are bonded with the OH^- group. The deconvolution of O 1 s exhibits two clear peaks located at binding energy at 529.6 eV and 530.5 eV, which is attributed to oxygen in the C-O of CoO crystal and Co_3O_4 crystal, respectively (Petitto et al. 2004; Wang et al. 2019). We transferred the specimen onto a heating chip to induce a heating pulse into the specimen. The morphology and structure of the nanosheets were investigated using high-resolution scanning transmission electron microscopy (HR-STEM). Figure 1c shows a high-resolution image of the synthesized nanosheet, which is visualized as an amorphous phase (Fig. 1d). When the heating pulse is applied to them, the amorphous nanosheets transform into crystalline cobalt particles above 500 °C (Fig. 1e).

When the temperature increases to 1100 °C, the nanosheets progressively transform as shown in Fig. 2a

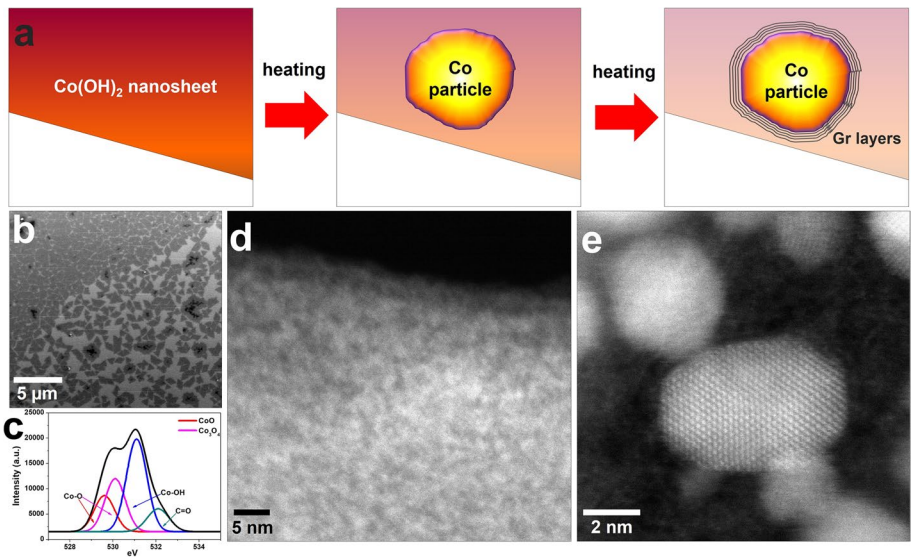

Fig. 1 **a** Simple schematic of the whole process. **b** and **c** SEM image and XPS spectra of the synthesized Co $(OH)_2$ nanosheets. **d** and **e** ADF-STEM images showing the nanosheet and Co particles formed using a heating holder

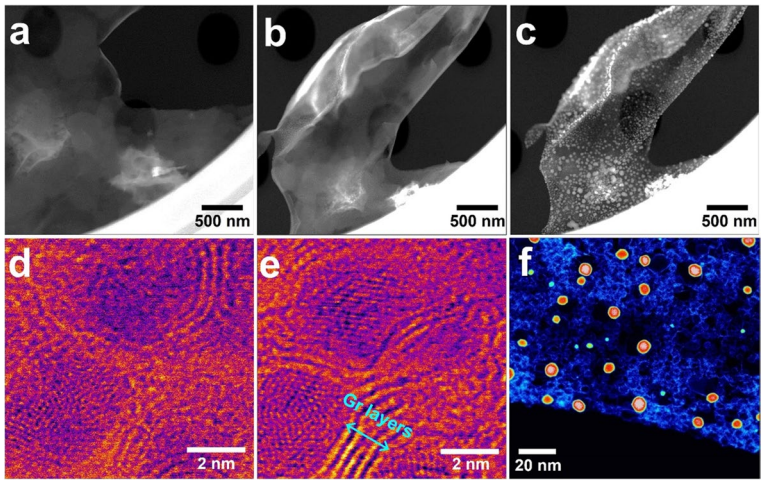

Fig. 2 **a**-**c** Successive HAADF-STEM images showing the transformation **d** and **e** BF-STEM images showing the Co particles with thin carbon film at 500 °C and 800 °C at the same position, respectively. **f** Low-scale HAADF-STEM images showing the Co particles with graphene layers

to c, which are successive high angle annular dark filed (HAADF)-STEM images showing the overall transformation behavior of the sheet in the same region. The transformation initiation is not implemented in only a specific area, but occurs in the entire sheet area to which temperature is applied, and Co atoms constituting Co $(OH)_2$ are aggregated to form a large amount of Co particles. When heated to 500 °C, Co particles are formed as shown in Fig. 1, and the hydrocarbons remaining on the surface of the Co $(OH)_2$ nanosheet form a thin film as shown in Fig. 2c. Figure 2d shows the bright filed (BF)-STEM image of the Co particles with a thin carbon film at 500 °C. Above 800 °C, the carbon film begins to crystallize gradually, and carbon layers (graphene layers) are formed at the edge of the Co particle (Fig. 2e). The Co particles encapsulated by graphene layers are visualized in Fig. 2f.

We observed an encapsulated Co particle using STEM mode, which allows us to collect various images using bright field (BF), annular dark field (ADF: DF2, DF4), and HAADF detectors simultaneously. Even if the material is composed of the same element, the degree of visualization differs depending on the type of detector used in STEM mode. This is because the detection degree of the scattered electron beam varies according to the scattering angle of the electron beam as it scatters through the material. Therefore, we obtained BF, DF2, DF4, and HAADF images in STEM mode to investigate the morphology and structure of a Co particle encapsulated by graphene layers as shown in Fig. 3. The distance between the graphene interlayers is measured to be 0.142 nm, which is consistent with the graphene interplanar spacing.

The graphene layer forms to surround the Co particles, and even if the Co particles partially move, the graphene layer maintains its shape. As shown in Fig. 4a, four graphene layers surround the Co particles, and they maintain their morphology while the Co particles move in the direction of the light blue arrow (Fig. 4b and c). This result suggests that the graphene layers surrounding the Co particles were not formed temporarily but were formed in a stacked form while maintaining the interlayer spacing with crystallinity. After EDS mapping confirmed the graphene layers remained after the movement of the Co particles, the graphene layers visualized in Fig. 4d and e were also included in the entire supported carbon film region, confirming the overall C mapping in the field of view.

The graphene layer surrounds the Co particles without a gap between the interface of the Co particles and the graphene layer. The number of graphene layers, which are observed prominently at 800 °C or higher, increases when a heating pulse of 1000 °C or higher is applied. Fig. 5 shows BF-STEM images of the graphene layers identified encapsulating the Co particle at 1050 °C. The number of graphene layers at the top of the Co particle was 9 (Fig. 5a), but when the results of continuous image acquisition were confirmed, the number of layers increased to 12 (Fig. 5b). In addition, the number of graphene layers surrounding the lower left part of the Co particle increased from 7 layers to 11 layers (Fig. 5c). This is because, as in the case of synthesizing graphene using a metal catalyst, Co particles act as a catalyst, and the remaining amorphous carbon source expands the number of graphene layers at 1000 °C or more and is smoothly crystallized into graphene. At

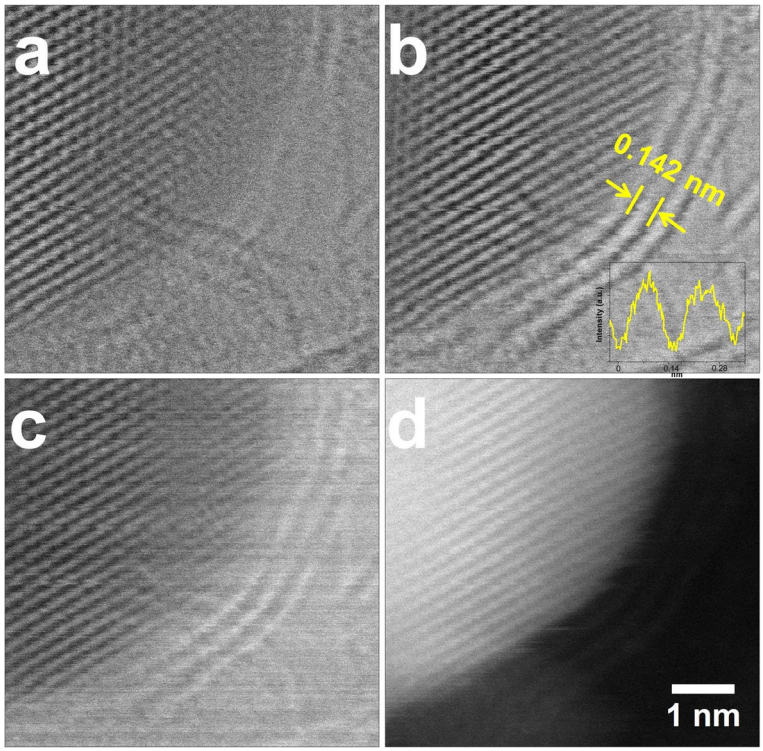

Fig. 3 Co particle encapsulated by graphene layers, which collected by (**a**) BF, (**b**) and (**c**) ADF and (**d**) HAADF detectors, respectively

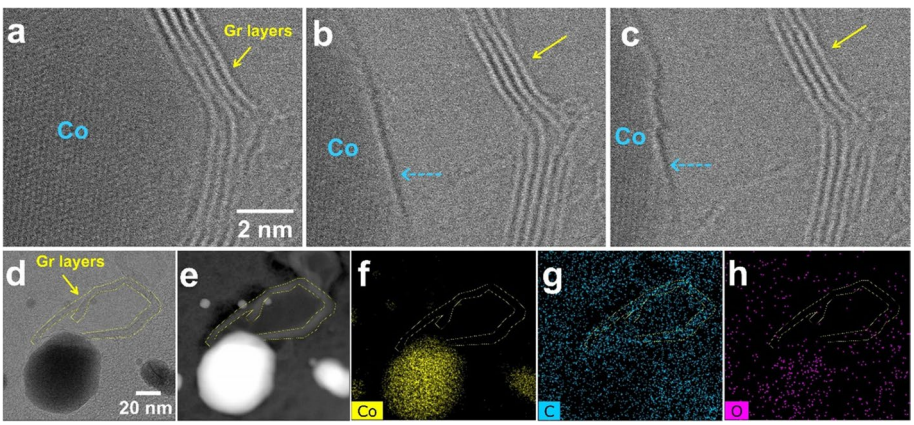

Fig. 4 **a**-**c** Successive BF-STEM images showing formation of graphene layers surrounding Co particle. **d**-**e** BF and HAADF-STEM images of Co particle and remaining graphene layers. **f**-**h** EDS mapping of Co, C, and O elements at the same region as (**d**) and (**e**)

another position, the growth process is also observed as shown in Fig. 5d-g.

Conclusions

We summarize that the behavior of Co particles encapsulated by graphene layers formed by high temperature and electron beam irradiation. The amorphous carbon remaining in the synthesized Co $(OH)_2$ nanosheet exists in the form of a thin film, which crystallizes when a temperature of 800 °C or higher is applied. The crystallized carbon grows into a graphene layer surrounding the Co particles, and the number of graphene layers gradually increases due to the catalytic activation of Co at temperatures above 1000 °C. All these behaviors were observed through STEM imaging, and the graphene layer composed of low elements was observed using BF and ADF

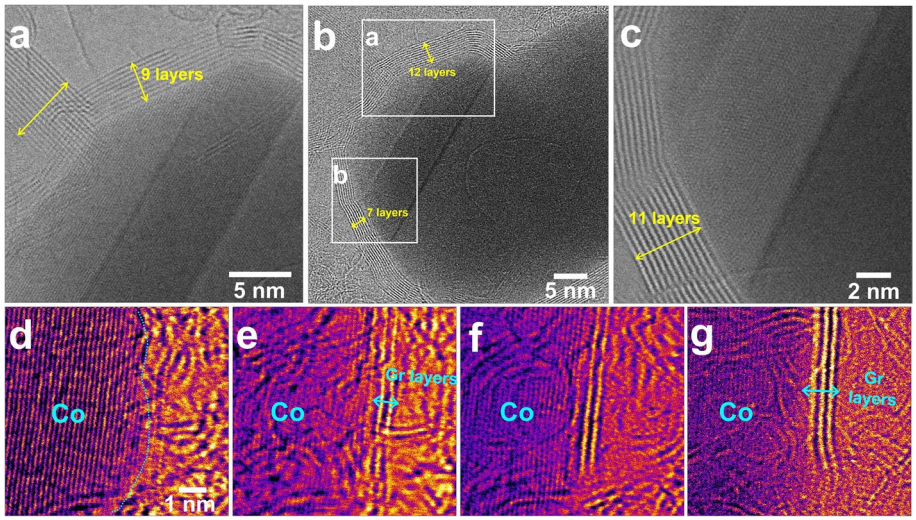

Fig. 5 **a**-**c** Successive BF-STEM images showing the growth of graphene layers at 1050 °C. **d**-**g** Successive BF-STEM images showing a initial states on the growth of graphene layers at another position

images in STEM mode, which has the advantage of using various detectors at the same time. The results of this work show a versatile and scalable technique that can be used to fabricate structured graphene materials.

Methods

Synthesis

Co $(OH)_2$ nanosheets were synthesized using the aqueous nutrient solution containing 2 mM cobalt nitrate hexahydrate and 2 mM hexamethylenetetramine (HMTA). Depending on the opening area of a container, a calculated amount of chloroform solution of sodium hexadecyl sulfate (SHS) was added to the water-air interface. After about 30 minutes, the container was capped and placed in a convection oven at 70 °C for typically 180 minutes. The synthesized Co $(OH)_2$ sheets were scooped using an TEM grid for imaging.

Transmission Electron microscopy

STEM images were acquired using an aberration-corrected FEI Titan Cubed TEM (FEI Titan3 G2 60–300), which was operated at a 200 kV acceleration voltage with a monochromator. Dose rate was 72.5 A/m^2.

Abbreviations

XPS: X-ray Photoelectron Spectroscopy; SEM: Scanning Electron Microscopy; HAADF-STEM: High Angle Annular Dark Field Scanning Transition Electron Microscopy; ADF: Annular Dark Field; BF: Bright Field; DF: Dark Field.

Acknowledgments

This work was supported by the National Research Foundation of Korea (NRF) grant funded by the Korea government (MSIT) (No. 2020R1G1A1099542) and Institute for Basic Science (IBS-R019-D1). This result was supported by "Regional Innovation Strategy (RIS)" through the National Research Foundation of Korea (NRF) funded by the Ministry of Education (MOE). (2021RIS-003).

Authors' contributions

Corresponding E-mail Address: gh.ryu@gnu.ac.kr. The author(s) read and approved the final manuscript.

Funding

This research received no external funding.

Availability of data and materials

The datasets used and/or analyzed during the study are available from the corresponding author on reasonable request.

Declarations

Competing interests

The authors declare that they have no competing interests.

Author details

[1]School of Materials Science and Engineering, Gyeongsang National University, Jinju 52828, Republic of Korea. [2]Department of Materials Science and Engineering, Ulsan National Institute of Science and Technology (UNIST), Ulsan 44919, Republic of Korea. [3]Center for Multidimensional Carbon Materials, Institute for Basic Science (IBS), Ulsan 44919, Republic of Korea.

Received: 18 May 2022 Accepted: 5 July 2022
Published online: 14 July 2022

References

F. Abild-Pedersen, J.K. Nørskov, J.R. Rostrup-Nielsen, J. Sehested, S. Helveg, Mechanisms for catalytic carbon nanofiber growth studied by ab initio density functional the- ory calculations. Phys. Rev. B **73**, 1 (2006). https://doi.org/10.1103/PhysRevB.73.115419

L. Chen, H. Chen, R. Luque, Y. Li, Metal–organic framework encapsulated Pd nanoparticles: Towards advanced heterogeneous catalysts. Chem. Sci. **5**, 3708 (2014). https://doi.org/10.1039/C4SC01847H

R. Chinchilla, C. Nájera, The sonogashira reaction: A booming methodology in synthetic organic chemistry. Chem. Rev. **107**, 874 (2007). https://doi.org/10.1021/cr050992x

A. Corma, P. Serna, P. Concepción, J.J. Calvino, Transforming nonselective into chemoselective metal catalysts for the hydrogenation of substituted nitroaromatics. J. Am. Chem. Soc. **130**, 8748 (2008). https://doi.org/10.1021/ja800959g

W.M. Czaplik, J.-M. Neudörfl, A.J. v Wangelin, On the quantitative recycling of Raney–Nickel catalysts on a lab-scale. Green Chem. **9**, 1163 (2007). https://doi.org/10.1039/B708057C

M.R. Friedfeld, M. Shevlin, J.M. Hoyt, S.W. Krska, M.T. Tudge, P.J. Chirik, Cobalt precursors for high-throughput discovery of base metal asymmetric alkene hydrogenation catalysts. Science **342**, 1076 (2013). https://doi.org/10.1126/science.1243550

V.R. Galakhov, A.S. Shkvarin, A.S. Semenova, M.A. Uimin, A.A. Mysik, N.N. Shchegoleva, A. Ye, E.Z. Yermakov, Kurmaev., Characterization of carbon-encapsulated nickel and iron nanoparticles by means of X-ray absorption and photoelectron spectroscopy. J. Phys. Chem. **C 114**, 22413 (2010). https://doi.org/10.1021/jp106612b

Y. Gamo, A. Nagashima, M. Wakabayashi, M. Terai, C. Oshima, Atomic structure of monolayer graphite formed on Ni(111). Surf. Sci. **374**, 61 (1997). https://doi.org/10.1016/S0039-6028(96)00785-6

D. Ge, L. Hu, J. Wang, X. Li, F. Qi, J. Lu, X. Cao, H. Gu, Reversible hydrogenation–oxidative dehydrogenation of quinolines over a highly active Pt nanowire catalyst under mild conditions. Chem Cat Chem **5**, 2183 (2013). https://doi.org/10.1002/cctc.201300136

A. Gruneis, D.V. Vyalikh, Tunable hybridization between electronic states of graphene and a metal surface. Phys. Rev. B **77**, 93401 (2008). https://doi.org/10.1021/acs.jpcc.5b05428

A.S.K. Hashmi, C.an Lothschütz, R. Döpp, M. Rudolph, T. D. Ramamurthi, F. Rominger., Gold and palladium combined for cross-coupling. Angew. Chem. Int. Ed. **48**, 8243 (2009). https://doi.org/10.1021/ja400311h

R.V. Jagadeesh, H. Junge, M.-M. Pohl, J. Radnik, A. Brückner, M. Beller, Selective oxidation of alcohols to esters using heterogeneous Co_3O_4–N@C catalysts under mild conditions. J. Am. Chem. Soc. **135**, 10776 (2013b). https://doi.org/10.1021/ja403615c

R.V. Jagadeesh, A.-E. Surkus, H. Junge, M.-M. Porl, J. Radnik, J.R. Rabeah, H. Huan, V. Schünemann, A. Brückner, M. Beller, Nanoscale Fe_2O_3-based catalysts for selective hydrogenation of nitroarenes to anilines. Science **342**, 1073 (2013a). https://doi.org/10.1126/science.1242005

Y. Le, X. Xu, P. Zhang, Y. Gong, H. Li, Y. Wang, Highly selective Pd@mpg-C_3N_4 catalyst for phenolhydrogenation in aqueous phase. RSC Adv. **3**, 10973 (2013). https://doi.org/10.1039/C3RA41397G

R. Liu, S.M. Mahurin, C. Li, R.R. Unocic, J.C. Idrobo, H. Gao, S.J. Pennycook, S. Dai, Dopamine as a carbon source: The controlled synthesis of hollow carbon spheres and yolk-structured carbon nanocomposites. Angew. Chem. Int. Ed. Engl. **50**, 6799 (2011). https://doi.org/10.1002/anie.201102070

Y.L. Liu, X.Y. Xu, P.C. Sun, T.H. Chen, N-doped porous carbon nanosheets with embedded iron carbide nanoparticles for oxygen reduction reaction in acidic media. Int. J. Hydrog. Energy **40**, 4531 (2015). https://doi.org/10.1039/C6RA27826D

A. Meffre, B. Mehdaoui, V. Connord, J. Carrey, P.F. Fazzini, S. Lachaize, M. Respaud, B. Chaudret, Complex nano-objects displaying both magnetic and catalytic properties: A proof of concept for magnetically induced heterogeneous catalysis. Nano Lett. **15**, 3241 (2015). https://doi.org/10.1021/acs.nanolett.5b00446

A. Nagashima, N. Tejima, C. Oshima, Electronic states of the pristine and alkali-metal-intercalated monolayer graphite/Ni(111) systems. Phys. Rev. B **50**, 17487 (1994). https://doi.org/10.1103/PhysRevB.50.17487

S.C. Petitto, M.A. Langell, Surface composition and structure of Co3O4(110) and the effect of impurity segregation. J. Vac. Sci. Technol. A **22**, 1690 (2004). https://doi.org/10.1116/1.1763899

R. Rahi, M. Fang, A. Ahmed, R.A. Sánchez-Delgado, Hydrogenation of quinolines, alkenes, and biodiesel by palladium nanoparticles supported on magnesium oxide. Dalton Trans. **41**, 14490 (2012). https://doi.org/10.1039/C2DT31533E

D. Ren, L. He, R.-S. Ding, Y.-M. Liu, Y. Cao, H.-Y. He, K.-N. Fan, An unusual chemoselective hydrogenation of quinoline compounds using supported gold catalysts. J. Am. Chem. Soc. **134**, 17592 (2012). https://doi.org/10.1021/ja3066978

R. Rosei, S. Modesti, F. Sette, C. Quaresima, A. Savoia, P. Perfetti, Electronic structure of carbidic and graphitic carbon on Ni(111). Phys. Rev. B **29**, 3416 (1984). https://doi.org/10.1103/PhysRevB.29.3416

G.M. Sammis, H. Danjo, E.N. Jacobsen, Cooperative dual catalysis: Application to the highly enantioselective conjugate cyanation of unsaturated imides. J. Am. Chem. Soc. **126**, 9928 (2004). https://doi.org/10.1021/ja046653n

H. Tian, X. Li, L. Zeng, J. Gong, Recent advances on the design of group VIII base-metal catalysts with encapsulated structures. ACS Catal. **5**, 4959 (2015). https://doi.org/10.1021/acscatal.5b01221

M. Toyofuku, S.-i. Fujiwara, T. Shin-ike, H. Kuniyasu, N. Kambe. Platinum-catalyzed intramolecular vinylchalcogenation of alkynes with β-phenylchalcogeno conjugated amides. J. Am. Chem. Soc. 130, 10504 (2008). https://doi.org/10.1021/ja804121j

S.-G. Wang, X.Y. Liao, D.B. Cao, Y.W. Li, J. Wang, H. Jiao, Formation of carbon species on Ni(111): Structure and stability. J. Phys. Chem. C **111**, 10894 (2007). https://doi.org/10.1021/jp070608v

Y. Wang, Y. Shi, Z. Zhang, C. Carlos, C. Zhang, K. Bhawnani, J. Li, J. Wang, P.M. Voyles, I. Szlufarska, X. Wang, Bioinspired synthesis of quasi-two-dimensional monocrystalline oxides. Chem. Mater. **31**(21), 9040 (2019). https://doi.org/10.1021/acs.chemmater.9b03307

Z. Wei, Y. Chen, J. Wang, D. Su, M. Tang, S. Mao, Y. Wang, Cobalt encapsulated in N-doped graphene layers: an efficient and stable catalyst for hydrogenation of quinoline compounds. ACS Catal. **6**, 5816 (2016). https://doi.org/10.1021/acscatal.6b01240

Z. Wei, J. Wang, S. Mao, D. Su, H. Jin, Y. Wang, F. Xu, H. Li, Y. Wang, In situ-generated Co_0-Co_3O_4/N-doped carbon nanotubes hybrids as efficient and chemoselective catalysts for hydrogenation of nitroarenes. ACS Catal. **5**, 4783 (2015). https://doi.org/10.1021/acscatal.5b00737

X. Wu, H. niu, S. Fu, J. Song, C. Mao, S. Zhang, D. Zhang, C. Chen., Core–shell CeO_2@C nanospheres as enhanced anode materials for lithium ion batteries. J. Mater. Chem. A **2**, 6790 (2014). https://doi.org/10.1039/C3TA15420C

M. Yan, T. Jin, Q. Chen, H.E. Ho, T. Fujita, L.-Y. Chen, M. Bao, M.-W. Chen, N. Asao, Y. Yamamoto, Unsupported nanoporous gold catalyst for highly selective hydrogenation of quinolines. Org. Lett. **15**, 1484 (2013). https://doi.org/10.1021/ol400229z

S. Yang, L. Peng, E. Oveisi, S. Bulut, D.T. Sun, M. Asgari, O. Trukhina, W.L. Queen, MOF-derived cobalt phosphide carbon nanocubes for selective hydrogenation of nitroarenes to anilines. Chem. Eur. J. **24**, 4234 (2018). https://doi.org/10.1002/chem.201705400

Y. Yao, Q. Fu, Y.Y. Zhang, X. Weng, H. Li, M. Chen, L. Jin, A. Dong, R. Mu, P. Jiang, L. Liu, H. Bluhm, Z. Liu, S.B. Zhang, X. Bao, Graphene cover-promoted metal-catalyzed reactions. Proc. Natl. Acad. Sci. U. S. A. **111**, 17023 (2014). https://doi.org/10.1073/pnas.1416368111

U.L. Zhang, L. Wang, H.-C. Zhang, Y. Liu, H.-Y. Wang, Z.-H. Kang, S.-T. Lee, Graphitic carbon quantum dots as a fluorescent sensing platform for highly efficient detection of Fe^{3+} ions. RSC Adv. **3**, 3733 (2013). https://doi.org/10.1039/C3RA23410J

Publisher's Note